SUPPORTING INFORMATION

Fe-Phthalocyanine Nanoclusters on $La_{0.67}Sr_{0.33}MnO_3$ Ferromagnetic Substrate for Spintronics Application

Emilia Annese,*,†,‡ T. J. A. Mori,‡ P. Schio,‡ B. Rache Salles,¶ and J. C. Cezar‡

†*Centro Brasileiro de Pesquisas Físicas, Rio de Janeiro, Brazil*

‡*Laboratório Nacional de Luz Síncrotron - Centro Nacional de Pesquisa em Energia e Materiais - CP 6192, 13083-970, Campinas, SP, Brazil*

¶*Instituto de Física, Universidade Federal do Rio de Janeiro (UFRJ)*

E-mail: emiliaannese@gmail.com

$SrTiO_3$: the substrate

All the heterostructures, presented in this work, were prepared on $SrTiO_3$ substrates (Mateck GmbH). A special care is needed to mount the substrate on the sample holder, to improve the electrical contact. In particular, tantalum wire were spot welded on the sample holder and always in contact with the substrate surface. Despite this care, the characterization made by X-ray photoemission may suffer of charging effect that induces at minimum a shift in the binding energy of the spectra. Two substrates were mounted on the same sample holder and a set of masks was used in order to differentiate the FePc thickness on the top of the substrate.[1]

$La_{0.67}Sr_{0.33}MnO_3/SrTiO_3$

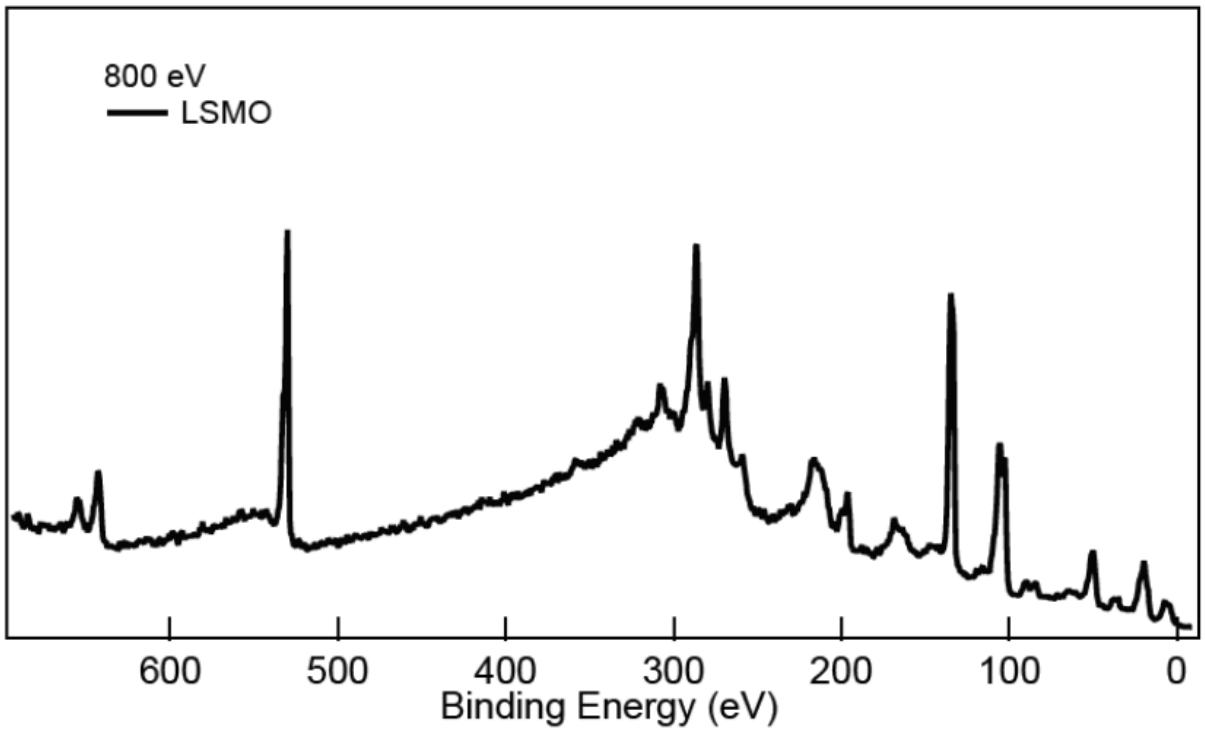

Figure S1: PE spectra at 800 eV measured on LSMO thin film.

The adsorption of Fe-Phthalocyanine (FePc) on $La_{0.67}Sr_{0.33}MnO_3$ (LSMO) is driven by different factors: oxide film morphology as well stoichiometry. Figure S1 displays the PE spectrum of pristine LSMO measured at 800 eV, whose analysis gives at once the La, Sr, Mn, O concentration at film surface. The spectrum binding energy alignment was done by using the La 4d peak. The quantitative analysis was performed by CASA-XPS. We accounted for cross-section of element transition at 800 eV to evaluate the concentration of each elements and ratio (table S1). A different concentration at surface is expected in correspondence of MnO_2 and (La,Sr)O terminations. In the table S1 the theoretical value were calculated from perfect stoichiometry of LSMO and does not take into account surface termination. (La,Sr)O is the most probable surface plane of LSMO film and there is C contamination (evaluated as C/O ratio). Both LSMO 90 nm and 60 nm tick films were characterized *in situ* and present similar morphology (AFM images), surface magnetic properties (XMCD) and stoichiometry

Table S1: Stoichiometry of $La_{0.67}Sr_{0.33}MnO_3$ surface.

	Mn 2p %	O1s %	Sr 3d %	La 4d %	Mn/O	Sr/La	C/O
theoretical	0.2	0.6	0.066	0.134	0.33	0.5	0
experimental	0.1	0.6	0.15	0.14	0.2	1	1.2

(XPS analysis) within the error bar.

These films present similar morphology, surface termination and magnetic properties.

Metal/organic/oxide deposition step: X-ray photoemission outlook

The heterostructures were characterized by X-ray photoemission at each deposition step. Figure S2 shows the PE spectra at 520 eV (a), 800 and 900 eV (b) for pristine LSMO film, FePc nano/LSMO and Co/FePc nano/LSMO, respectively. The binding energy alignment of PE spectrum was done by using the La 4d peak. This energy correction works in the case of pristine LSMO and FePc nano/LSMO samples, but does not in the case of Co/FePc nano/LSMO. The Co deposition on FePc nano/LSMO heterostructure is not expected to produce such charging effect, since its metallic nature. However, this is a further proof of the Co spatial and electron confinement in between FePc nanoclusters.

PE spectrum of FePc nano/LSMO shows N 1s and C 1s spectral fingerprint. To account for the C contaminant, high resolution PE spectrum of pristine LSMO film was acquired and subtracted from the spectrum FePc nano/LSMO (main text of the manuscript).

Upon Co deposition we observed well distinct spectral features: Co 2p, Co 3p and typical Co VB band at Fermi level, beside the binding energy shift observed due to possible charge dipole at the surface. To understand the composition of the heterostructure upon subsequent deposition of molecules and Co we evaluate the ratio of between PE intensity of organic part of the molecule (C,N) and element of the (La,Sr)O surface and Co (table S2).

To evaluate the correct C content related to FePc molecule we subtracted the intensity

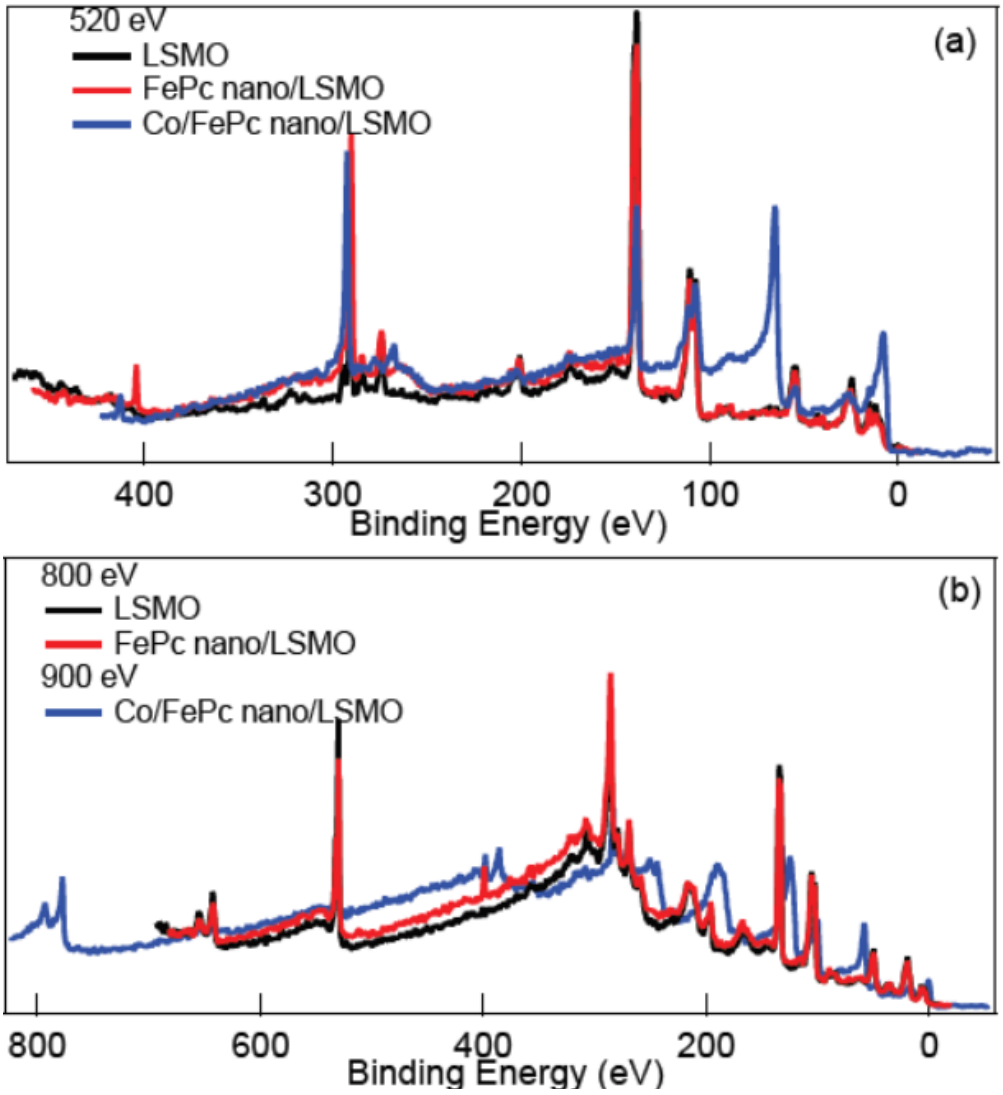

Figure S2: PE spectra at 520 (a), 800 and 900 eV (b) acquired at each deposition step: pristine LSMO (black line), FePc nano/LSMO (red line) and Co/FePc nano/LSMO (blue line).

of C 1s PE signal of pristine LSMO film from the one of FePc nano/LSMO. From the semi quantitative analysis of PES data, we observed the relative content of each element at the surface.

Table S2: The relative content of each element calculated as the ratio of the organic part (C, N) and the one of supporting surface plane (La, Sr, O) and Co metal.

deposition	C/N	C/Sr	C/O	Co/C	Co/N	Co/O	Co/Sr	Co/La
FePc	7(1)	3(0.1)	0.73(5)					
Co				1.4(7)	4.0(5)	1.5(1)	5(1)	3.0(1)

FePc cluster formation vs. FePc evaporation rate

Table S3 summarizes the hybrid organic/inorganic interfaces investigated in this work. For

Table S3: Hybrid heterostructure preparation conditions. FePc deposition rate obtained from a quartz micro balance.

higher FePc deposition rate: 0.14 nm/min — LSMO thickness: 90 nm		
Sample label	t_{FePc}(nm)	t_{Co} (nm)
H1	1.4	0.5
lower FePc deposition rate: 0.06 nm/min — LSMO thickness: 60 nm		
L2	1.2	–
L3	1.4	–
L4	0.5	–
L5	0.1	–
Co — LSMO thickness: 60 nm		
01	–	0.5

FePc layers around 1.5 nm thick, we observed a dependence on the evaporation rate. Figure S3 (a,b) shows the morphology of FePc cluster formation for two different deposition rates: 0.14 nm/min (a) and 0.06 nm/min (b). By reducing the evaporation rate the average cluster diameter changes from ∼20(5) nm to ∼10(5) nm and from 3(0.5) to 0.7(5) nm in cluster height. Samples grew at lower deposition rate also presented a more uniform distribution on the LSMO surface. In the main text we referred to samples H1, L2 and L3, as FePc nanoclusters/LSMO. These are the samples with effective thickness above 1 nm, which leads to molecules nanoparticles where most of the Fe atoms are in a bulk-like situation. Samples L4 and L5 are referred as FePc/LSMO once that given their effective thickness around 0.4 nm, most of the Fe in the molecules are in direct contact with the LSMO buffer layer.

FePc orientation within the nanoclusters

Figure S4 (a,f) displays the N K and Fe L_3 edges XAS data for FePc at LSMO interface and within the nanocluster (as deposited with a rate of 0.06 nm/min) at normal (0°) and grazing (55°) incidence. In the case of N XAS data, the $1s \rightarrow 2p$ transition is toward π^* and

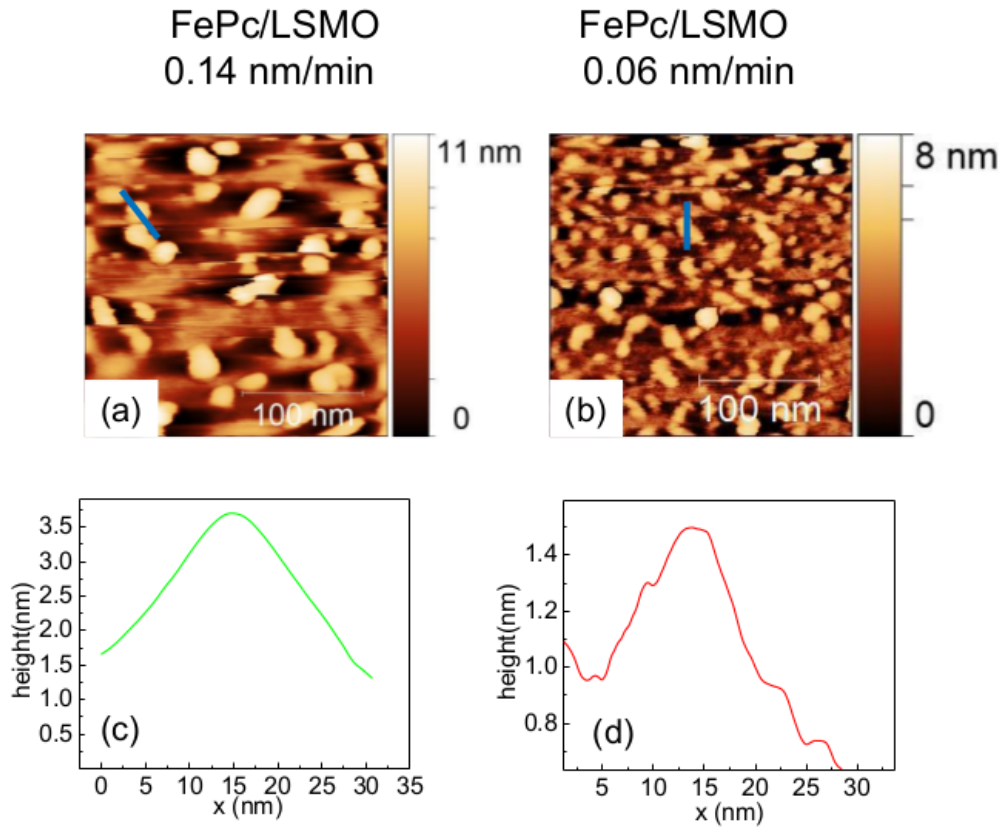

Figure S3: AFM image of FePc cluster formation on $La_{0.66}Sr_{0.33}MnO_3$ obtained with two different FePc deposition rates: 0.14 nm/min (a) and 0.06 nm/min (b). (c-d) The AFM profiles of panels (a) and (b).

σ^* states below and above 405 eV, respectively. The spectrum alignment was made using La 3d peaks that appears (at 425 eV) as second order effect of undulator harmonics in XAS. In the π^* region the features at the lowest energies correspond to N atoms in N_1 and N_2 sites (FigureS4). The N K edge line shape does not vary for θ= 0 and 55 ° indicating a random orientation of the molecules within the nanoclusters.

Fe L_3 XAS data probe the unoccupied s and d states of the molecule projected to the Fe site. The Fe 3d band of bulk-like is split by a molecular field of D_{4h} symmetry and the occupation of 3 d orbitals depends on the temperature and ligand.[2] Once the molecules organize on a substrate, the interaction with the latter induces a redistribution of 3d occupancy.[3] Both Fe L_3 spectra measured at θ= 0 and 55 ° on FePc within the nanoclusters show similar line shape characterized by electronic distribution characteristic of thin FePc deposited on

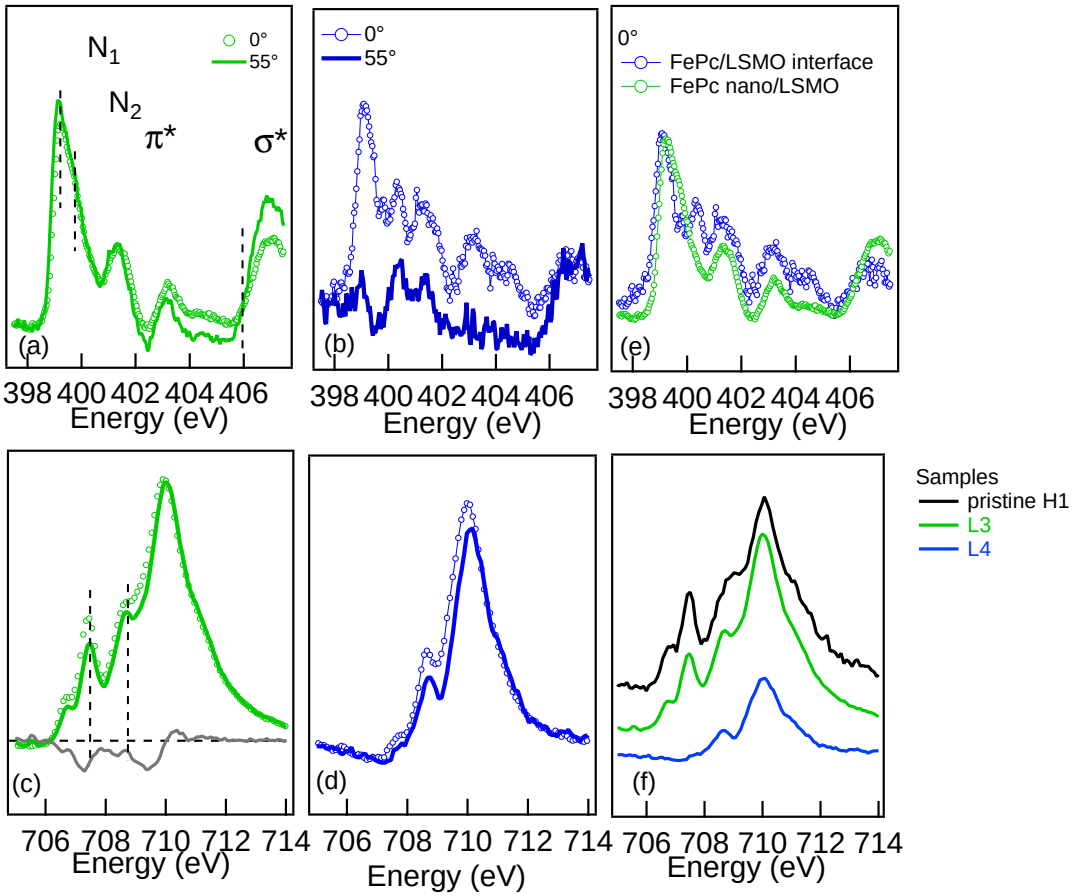

Figure S4: Left side: **Top**: FePc molecule scheme; **Bottom**: Geometry of XAS experiment: p–type X-ray polarization belongs to the plane identified by incoming beam direction and sample surface normal and X-ray beam can be rotated from normal (0°) to grazing incidence ($\sim$ 55°). Right side: XAS spectra at N K (a-b,e) and Fe L_3 (c-d,-f) edges were measured: at 0° (circles) and at =55° (continuous line) and at RT. In N K XAS spectra the energy characteristic for the two N sites in FePc are highlighted. Panels (e-f) show N K (a-b,e) and Fe L_3 XAS line shape modification going from FePc at the interface (blue) to FePc in the nanoclusters (black and green).

substrate as in Ref. 4 and associated to FePc ^3E_g ground state. The negligible dichroism at both N K and Fe L_3 edges also indicates the random orientation of the molecules. The self-assembling of organic molecule on metal, semimetal and oxide depends on the relative strength of intermolecular and molecule/substrate interaction. On one hand, it is known that MPc adsorb flat on the metal surface as reported in this Ref. 5 where the interaction of MPc on different metal surface is reviewed. MPc adsorbs flat lying on some oxides (MnO,

MoO, TiOx) as already demonstrated in several studies (6,7). This usually indicates that the molecule/substrate interaction is prevailing against the intermolecular interaction. On the other hand, two different orientations of the same planar molecules can be obtained depending on the starting surface $La_{0.67}Sr_{0.34}MnO_3$ or cobalt.[8] Surface termination, oxidization and roughness may have a role in the molecule self-organization. In our case, we followed each step of the heterostructure preparation (LSMO surface roughness as small as 0.1 Å and surface termination with La(SrO) plane) and verified that as in the case of double-decker phthalocyanine, FePc is almost standing up on LSMO surface. As far as the FePc content increase, the molecule self-arrange randomly creating nanocluster of nm size.

Fe X-ray absorption:CTM4XAS calculations

Experimental XAS data are compared with crystal field multiplet calculations using the CTM4XAS interface.[9] The Fe $L_{2,3}$ spectra are calculated from the sum of all possible transitions for an electron excited from the 2p core level into an unoccupied 3d level. The ground state is approximated by the electronic configuration 3d. Calculation account for the crystal field effect and spin orbit interaction in 3d ground state and for dd, pd multiple coupling in the final states. Empirical parameters such as 10Dq, Ds, and Dt indicates the crystal field strength and are optimized to reproduce the experimental results. The calculated spectra include a Lorentzian FWHM of 0.2 (0.4) eV for the $2p_{3/2}$ ($2p_{1/2}$) core level to account for intrinsic line width broadening, and a Gaussian FWHM of 0.1 eV for instrumental broadening. To easily compare the line shapes, both experimental and theoretical spectra are aligned in energy with respect to the peak with maximum intensity. XAS spectra simulation were performed by using the parameters reported in the table S4. The electronic configuration of Fe and Co were established from the calculations and Refs[2,4,10,12–15]

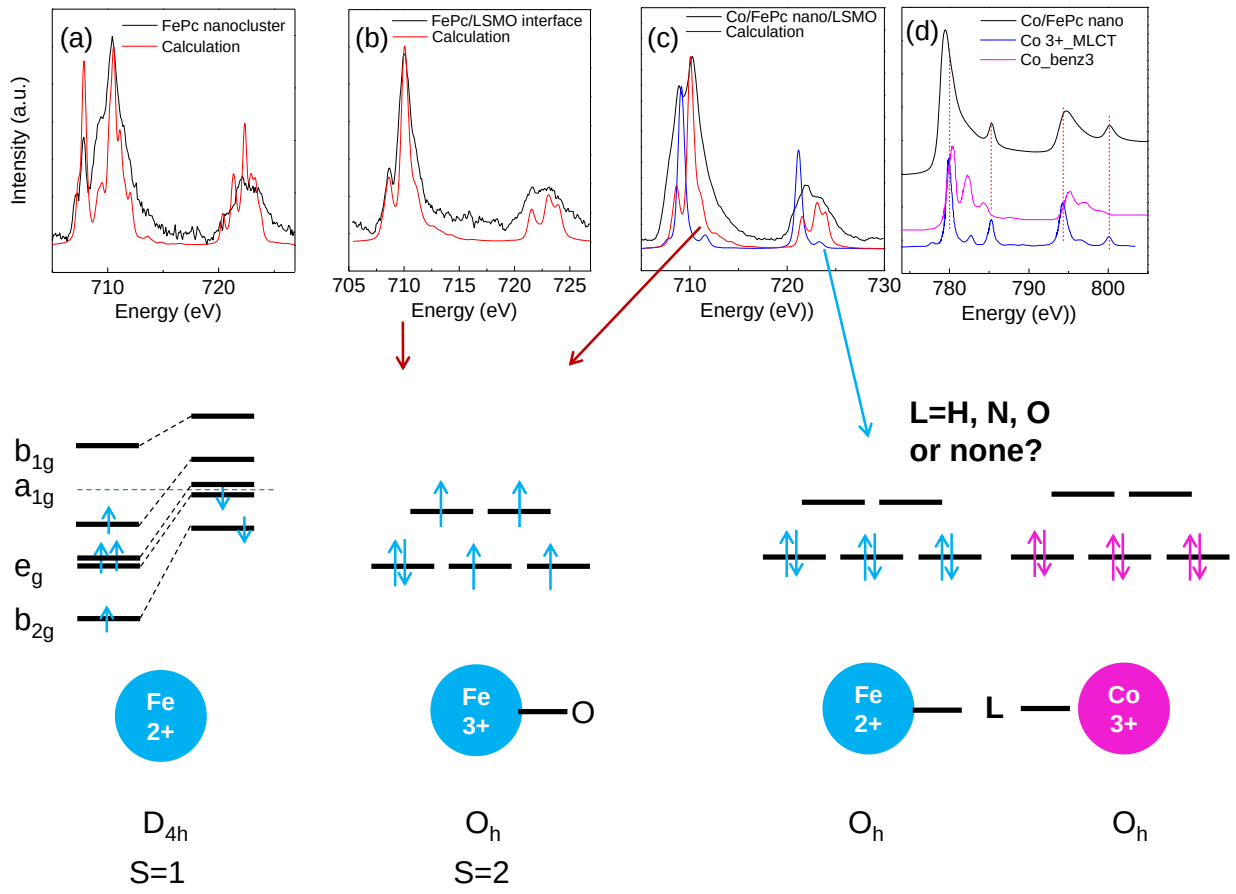

Figure S5: Experimental XAS data and calculations are given for: FePc in nanoclusters (a), FePc at interface (b), FePc after Co deposition at Fe (c) and Co L $_{2,3}$ edges (d). The spectra measured at 300 K, but for the one at Co $L_{2,3}$ edges measured at 10 K. The simulation were made within ligand field approximation accounting for crystalline electronic field, spin-orbit coupling and charge transfer. In the case of Co, the metal to ligand charge transfer calculation was reproduced from Ref 10 (blue line). As a further term of comparison the Co spectra of Co nanocluster surrounded by three benzene rings from Ref 11 (magenta line). At the bottom, the electronic configuration corresponding to each panel: Fe^{2+} in D_{4h} symmetry as in Refs 2,4,12, weakly interacting molecule; Fe^{3+} in O_h symmetry, FePc in contact with oxidized interface; mixed Fe configuration upon Co deposition: Fe^{2+}, Fe^{3+} and Co^{3+} in O_h symmetry.

Co/FePc nano/LSMO: Co X-ray absorption spectrum versus temperature

In the heterostructure Co may be surrounded by other Co atoms, by FePc molecules and by LSMO surface, each environment having characteristic signature discernible in XAS and

Table S4: In the calculations we account for: octahedral O_h or tetrahedral D_{4h} symmetry and its extent in 10 D_q, D_s, D_t and charge transfer, CT.

sample	element	O_h–10 D_q	D_{4h}–10 D_q	Ds	D_t	CT
FePc nano	Fe	–	2.6	1.08	0.25	0
FePc/LSMO	Fe	1	–	–	–	1
Co/FePc nano/LSMO	Fe	2.7	–	–	–	2

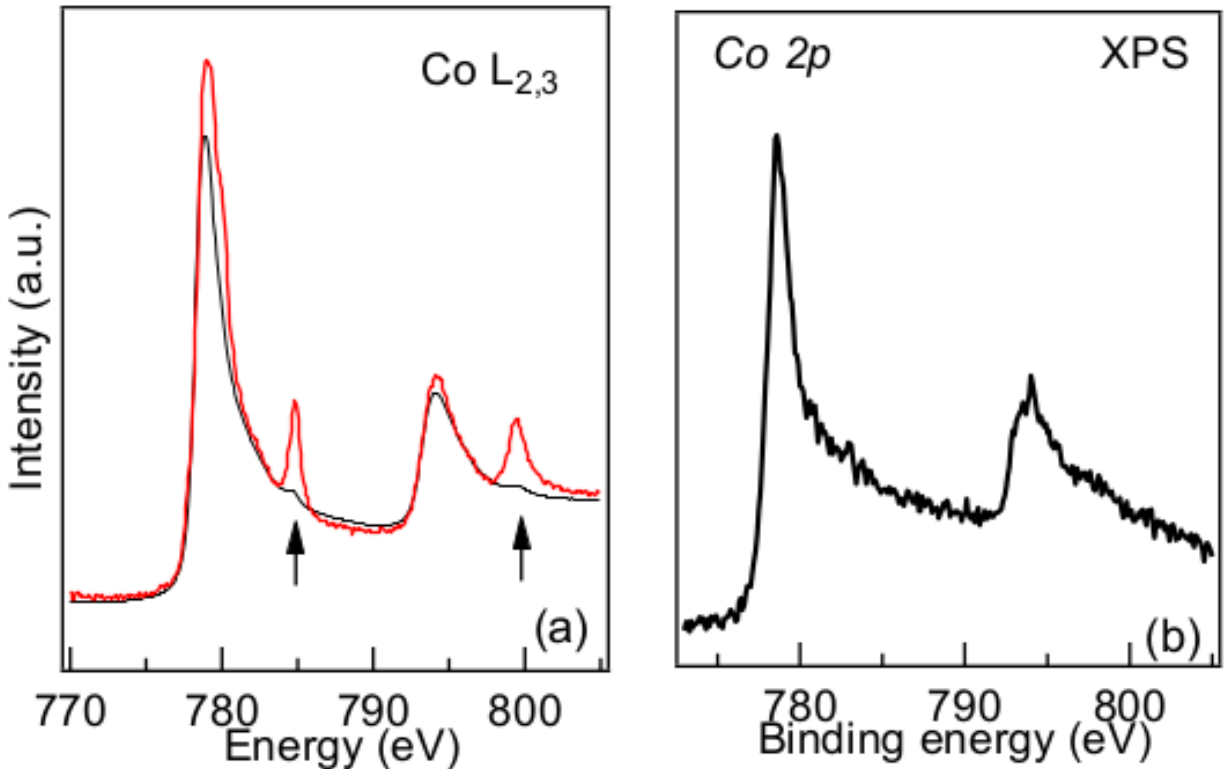

Figure S6: (a) Co $L_{2,3}$ X-ray absorption spectra measured at 300 and 10 K. (b) Co 2p core level sepectrum measured at RT.

XPS. The direct contact of Co with LSMO may induce Co oxide formation. XAS spectrum at Co L_3 provides information about the atom confinement within the organic matrix or in metallic by a variation in the spectral line shape. Figure S6 (a) shows Co $L_{2,3}$ X-ray absorption spectra measured at 300 and 10 K and (b) Co 2p core photoemission level. Co XAS spectral line shape resembles the one of metallic Co, but for features at 6 eV above $L_{2,3}$ edges, more prominent at low temperature. Among the possible interpretations of these features the most probable are: the formation of Co nanocluster embedded in the organic aromatic part of the molecule or inclusion of some Co atoms with FePc matrix forming a

bimetal molecule. In the case of nanocluster formation, it is already known that Co bond with benzene rings displays localized states in this energy region and detectable at low temperature.[11] This hypothesis could be supported from the bond formation between the Co and the atoms within the molecules (C, N) as inferred from the core level spectral line shape modification (Figure 3 (e,f) in the main text). However, the latter behavior is present even in the Co formation on top of FePc layers.[16]

On the other hand, the photoemission spectra of Co metal and Co oxides differs in the main core level ($2p_{3/2}$ and $2p_{1/2}$) binding energy position and presence of satellites (at $\sim$ 5 eV in CoO and at 10 eV in Co_3O_4) above both $2p_{3/2}$ and $2p_{1/2}$[17]. The measured Co 2p core level spectra do not show clear satellites in the this energy region.

Field Cooling curve simulation in presence of dipole interaction

Field Cooling (FC) magnetization curve of a superparamagnetic system is reproduced by the following equation:

$$M_{FC}(T) = \frac{H * M_s^2}{3K} ln\left(\frac{\tau_m}{\tau_0}\right) \times \left[\int_0^T \frac{T_B}{T} f(T_B) dT_B + \int_T^\infty f(T_B) dT_B\right] \quad (1)$$

where H is the magnetic field, M_s is the saturation magnetization and K the effective magnetic anisotropy and f is the blocking temperature distribution due to size distribution, in this case a log-normal distribution. In the low field approximation the first integral is the magnetic contribution of the nanoparticles in the superparamagnetic regime (T_B <T) whereas the second integral is the contribution of the blocked magnetic moment (T_B >T). We assume that the temperature dependence of the spontaneous magnetization follows the

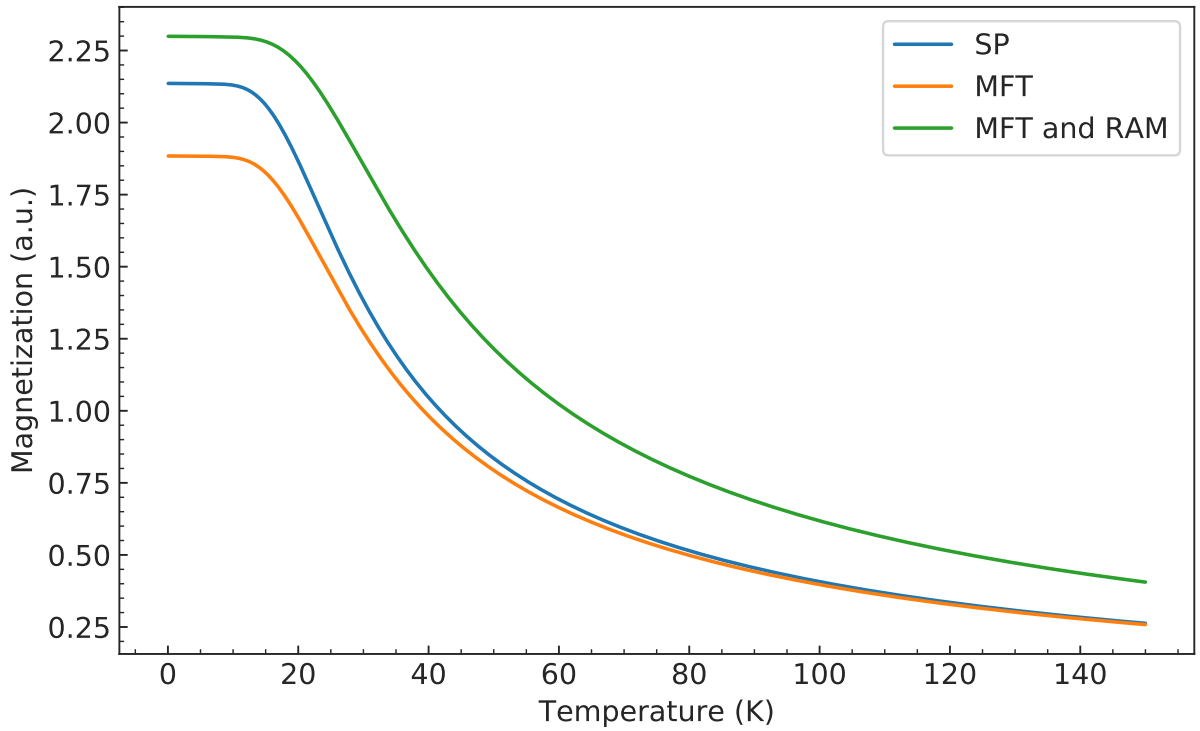

Figure S7: Field Cooling magnetization curves for a superparamagnetic model (blue) and for nanoparticles with dipolar interaction with the mean field theory (MFT - red), and with MFT and the random anisotropy model (MFT and RAM - green).

Bloch's law, given by

$$M_s(T) = M_{sp}(0)[1 - (T/T_C)^{3/2}] \tag{2}$$

where $M_{sp}(0)$ is the spontaneous magnetization at 0 K and T_C is the Curie temperature.[18]

In the mean field approximation (MFA), the dipolar interaction (DI) is introduced by adding an interaction field which depends on the magnetization as

$$H = H_{app} + \lambda M_{FC}(T)/M_{sp}(0) \tag{3}$$

where λ is a parameter that quantify the strength of the dipolar interaction. We thus obtain for the magnetization a self-consistent equation that is iteratively calculated.

The random anisotropy model (RAM) takes into account the collective behavior of closed packed randomly oriented magnetic nanoparticles in a nonmagnetic matrix. In this model,

Table S5: Value of the parameters used for the simulation of FC curve.

Approximation	T_c(K)	D(cm)	M_s(emu/g)	K(erg/cc)	C	A	x	λ(Oe)
MFA+RAM	1400	5.10^{-7}	80	2.1 e^4	100	5 e^{-10}	0.5	-100

the effective anisotropy K_eff of N interacting particle contained within a correlation length l is averaged to a value $K/\sqrt{N}$, analogue to the random walk distance after N steps. The number of interacting particles is given by

$$N = [1 + x(l^3 - d^3)/d^3] \tag{4}$$

where x is the density of nanoparticles and d is their diameter. The correlation length is given by

$$l = D + \sqrt{\frac{2A_{eff}}{M_s H + C}} \tag{5}$$

where A_{eff} and C are constants.

The calculations were done in python.

References

(1) Annese, E.; Mori, T. J. A.; Schio, P.; Salles, B. R.; Cezar, J. C. Applied Surface Science Influence of the growth parameters on the electronic and magnetic properties of La 0 . 67 Sr 0 . 33 MnO 3 epitaxial thin films. *Applied Surface Science* **2018**, *437*, 281–286.

(2) Kroll, T.; Kraus, R.; Schönfelder, R.; Aristov, V. Y.; Molodtsova, O. V.; Hoffmann, P.; Knupfer, M. Transition Metal Phthalocyanines: Insight into the Electronic Structure from Soft X-Ray Spectroscopy. *J. Chem. Phys.* **2012**, *137*, 054306–7.

(3) Annese, E.; Casolari, F.; Fujii, J.; Rossi, G. Interface Magnetic Coupling of Fe-Phthalocyanine Layers on a Ferromagnetic Surface. *Phys. Rev. B* **2013**, *87*, 054420–6.

(4) Bartolomé, J.; Bartolomé, F.; García, L. M.; Filoti, G.; Gredig, T.; Colesniuc, C. N.;

Schuller, I. K.; Cezar, J. C. Highly Unquenched Orbital Moment in Textured Fe-Phthalocyanine Thin Films. *Phys. Rev. B* **2010**, *81*, 195405–8.

(5) Peisert, H.; Uihlein, J.; Petraki, F.; Chassé, T. Charge transfer between transition metal phthalocyanines and metal substrates: The role of the transition metal. *Journal of Electron Spectroscopy and Related Phenomena* **2015**, *204*, 49 – 60.

(6) Glaser, M.; Peisert, H.; Adler, H.; Uihlein, J.; Nagel, P.; Merz, M.; Schuppler, S.; Chasse, T. Transition-Metal Phthalocyanines on Transition-Metal Oxides : Iron and Cobalt Phthalocyanine on Epitaxial MnO and TiO x Films. *J. Phys. Chem. C* **2015**, *119*, 27569–27579.

(7) Liu, L.; Zhang, W.; Guo, P.; Wang, K.; Wang, J.; Qian, H.; Kurash, I.; Wang, C.-h.; Yang, Y.-w.; Xu, F. A direct Fe – O coordination at the FePc / MoO x interface investigated by XPS and NEXAFS. *Phys.Chem.Chem.Phys.* **2015**, *17*, 3463–3469.

(8) Malavolti, L.; Poggini, L.; Margheriti, L.; Chiappe, D.; Graziosi, P.; Cortigiani, B.; Lanzilotto, V.; de Mongeot, F. B.; Ohresser, P.; Otero, E.; Choueikani, F.; Sainctavit, P.; Bergenti, I.; Dediu, V. A.; Mannini, M.; Sessoli, R. Magnetism of TbPc2 SMMs on ferromagnetic electrodes used in organic spintronics. *Chemical Communications* **2013**, *49*, 11506.

(9) Stavitski, E.; de Groot, F. M. The CTM4XAS program for EELS and XAS spectral shape analysis of transition metal L edges. *Micron* **2010**, *41*, 687–694.

(10) Bonhommeau, S.; Pontius, N.; Cobo, S.; Salmon, L.; De Groot, F. M.; Molnár, G.; Bousseksou, A.; Dürr, H. A.; Eberhardt, W. Metal-to-ligand and ligand-to-metal charge transfer in thin films of Prussian blue analogues investigated by X-ray absorption spectroscopy. *Physical Chemistry Chemical Physics* **2008**, *10*, 5882–5889.

(11) Akin, S. T.; Zamudio-Bayer, V.; Duanmu, K.; Leistner, G.; Hirsch, K.; Bülow, C.; Ławicki, A.; Terasaki, A.; von Issendorff, B.; Truhlar, D. G.; Lau, J. T.; Duncan, M. A.

Size-Dependent Ligand Quenching of Ferromagnetism in Co3(benzene) n + Clusters Studied with X-ray Magnetic Circular Dichroism Spectroscopy. *The Journal of Physical Chemistry Letters* **2016**, *7*, 4568–4575.

(12) Kuz'min, M. D.; Hayn, R.; Oison, V. *Ab initio* calculated XANES and XMCD spectra of Fe(II) phthalocyanine. *Phys. Rev. B* **2009**, *79*, 024413–5.

(13) Miedema, P. S.; Stepanow, S.; Gambardella, P.; De Groot, F. M. 2P X-Ray Absorption of Iron-Phthalocyanine. *Journal of Physics: Conference Series* **2009**, *190*, 012143–7.

(14) Miedema, P. S.; Schooneveld, M. M. V.; Knop-gericke, A.; Groot, F. M. F. D. Oxygen Binding to Cobalt and Iron Phthalocyanines As Determined from in Oxygen Binding to Cobalt and Iron Phthalocyanines As Determined from in Situ X-ray Absorption Spectroscopy. *Journal of Physical Chemistry C* **2011**, *115*, 25422–25428.

(15) Van Der Laan, G.; Kirkman, I. W. The 2p absorption spectra of 3d transition metal compounds in tetrahedral and octahedral symmetry. *Journal of Physics: Condensed Matter* **1992**, *4*, 4189–4204.

(16) Annese, E.; Di Santo, G.; Choueikani, F.; Otero, E.; Ohresser, P. The Formation of Metallic Ferromagnetic Thin Film on Top of FePc Ordered Thin Film: The Chemical and Magnetic Properties of the Interface. *The Journal of Physical Chemistry C* **2019**, *123*, 17521–17529.

(17) Gwag, J. S.; Sohn, Y. Interfacial natures and controlling morphology of Co oxide nanocrystal structures by adding spectator Ni ions. *Bulletin of the Korean Chemical Society* **2012**, *33*, 505–510.

(18) Hochepied, J.; Pileni, M. Magnetic properties of mixed cobalt–zinc ferrite nanoparticles. *Journal of Applied Physics* **2000**, *87*, 2472–2478.